Solar energetic particle analysis platform for the inner heliosphere

SERPENTINE

Cycle 25 Shocks Catalog

User documentation

UNIVERSITY OF TURKU

UNIVERSITÉ TOULOUSE III PAUL SABATIER

C A U Kiel University Christian-Albrechts-Universität zu Kiel

Imperial College London

HELSINGIN YLIOPISTO
HELSINGFORS UNIVERSITET
UNIVERSITY OF HELSINKI

Universidad de Alcalá

Contents

List of Figures

List of Tables

List of Acronyms

AU	Astronomical Unit
EPD	Energetic Particle Detector
EPT	Electron Proton Telescope
FF	Fast Forward
FR	Fast Reverse
HET	High Energy Telescope
ICME	Interplanetary Coronal Mass Ejection
IP	Interplanetary
MAG	Magnetometer
MC	Magnetic Coplanarity
MHD	MagnetoHydroDynamics
MX	Mixed Mode
PAS	Proton and Alpha Sensor
PSP	Parker Solar Probe
SC	spacecraft
SEP	Solar Energetic Particle
SERPENTINE	Solar energetic particle analysis platform for the inner heliosphere
SODA	ShOck Detection Algorithm
SolO	Solar Orbiter
STEP	SupraThermal Protons and alpha
STEREO	Solar Terrestrial Relations Observatory
SWA	Solar Wind Analyser
TRUFLS	Tracking and Recognition of Universally Formed Large-scale Shocks
ULF	Ultra Low Frequency
WP	Work Package

SUMMARY

Interplanetary (IP) shocks are fundamental building blocks of the heliosphere. A statistical approach to study the features and understand the behaviour of such important structures has proven invaluable in the past (e.g., Kilpua et al. 2015).

The SERPENTINE project provides the community with a statistical effort in this direction, providing shock identification and characterisation for shocks during Cycle 25. The focus is on events related to Solar Energetic Particle (SEP) events, representing another data product of the project (the Cycle 25 SEP catalog). The Cycle 25 shock catalog is publicly available at `https://data.serpentine-h2020.eu/`. This document provides the documentation to the catalog, making it clear for users to understand how shocks have been identified, what parameters are provided and how they are computed.

The catalog is organised in two subsets: a multi-SC list of shocks with characterisation in conjunction to SEP events, and a SolO shock list, tracking all the shocks observed with this SC and providing an enhanced level of characterisation, thus ensuring maximum exploitation of the novel SolO capabilities. Throughout this document, such a distinction (multi-SC – SolO list) is often used. Clearly, a subset of the SolO events participate to the multi-SC list.

The documentation following the data reduction pipeline sketched in Figure 1. We elucidate which spacecraft we use for the shock list in Section 1. In Section 2, we describe how shocks are identified within the catalogue. The shock characterisation strategy is described in Section 3. Finally, a streamlined description of the shocks catalog is shown in Section 4.

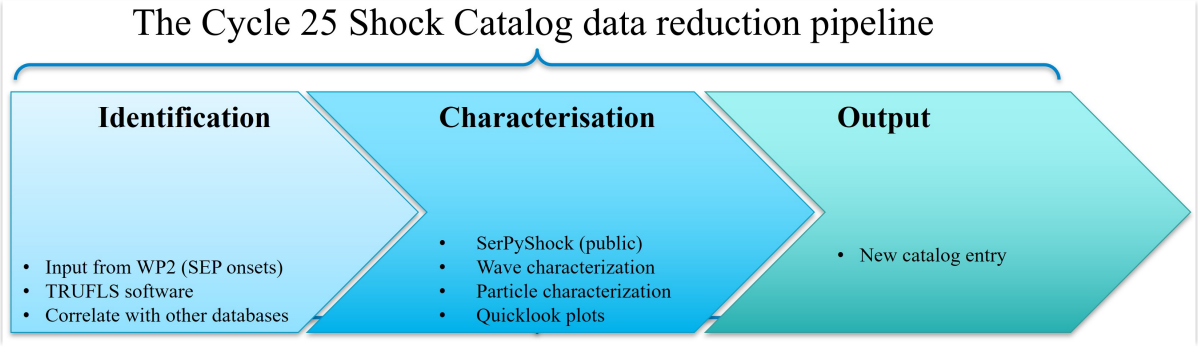

Figure 1: Sketch of the data reduction pipeline for the SERPENTINE cycle 25 shocks catalog

1 Datasets and missions

The multi-spacecraft (SC) list utilises data from Solar Terrestrial Relations Observatory (STEREO) and Wind. In both cases, the on-board magnetic field and plasma instruments are used. In the multi-SC shock list, shocks are searched in connection to the events contained in the Solar energetic particle analysis platform for the inner heliosphere (SERPENTINE) Cycle 25 Solar Energetic Particle (SEP) events catalog, thus adding further characterisation for the potential sources of particle acceleration. The shocks and SEP events are linked through clickable identifiers.

In the multi-SC list, events are searched for a time window of about 120 hours after the SEP onset time (detailed in the catalog as end and start time search). Therefore, some SEP events are linked to more than one shock while some other will have no associated in-situ shock.

The events are identified with the Tracking and Recognition of Universally Formed Large-scale Shocks (TRUFLS) code developed within SERPENTINE, soon to be released and described in Section 2 of this document.

The Wind events are always checked against the CfA interplanetary shock database (`https://lweb.cfa.harvard.edu/shocks/wi_data/`), to which we refer users that are particularly interested in stupying Interplanetary (IP) shocks using Wind. Similarly, for the study of shocks in the inner heliosphere using Parker Solar Probe (PSP),we direct the users to the novel ShOck Detection Algorithm (SODA) PSP catalog at `https://parker.gsfc.nasa.gov/shocks.html`.

In the Solar Orbiter (SolO) shock list we report all the IP shocks that crossed the spacecraft since launch, with the requirement that magnetic field and plasma data must available, even when there are no events in the SEP events in the catalog. Some magnetic field-only candidates from the early SolO mission have been included as they were reported elsewhere by the community. For SolO, Energetic Particle Detector (EPD) data has been used in addition to the plasma and magnetic field data.

2 Shock identification

Shocks are abrupt transitions between a supersonic (upstream) and a subsonic (downstream) flow, and can be viewed as discontinuities and, therefore, sudden changes in the plasma conditions. In this picture, to identify shocks and characterise their statistical properties in the large datasets provided by modern SC missions becomes a non-trivial task, due to the fact that the sudden changes in the plasma properties mentioned above happen on very small ($\sim$ seconds) timescales. Most of the shocks in the catalog are identified with the TRUFLS code developed within the SERPENTINE project and documented below (Section 2.1). Other means of identification are discussed in Section 2.2.

2.1 The TRUFLS code

The TRUFLS code is built to look at long time series and identify shocks automatically. An important, similar effort has been done for other SC missions in the Heliospheric Shock Database generated and maintained at the University of Helsinki; see `http://ipshocks.fi` and Kilpua et al. (2015) for further details. To compile such catalogue, the authors used either visual inspection of magnetic field and plasma data, or, for a small number of missions, a machine learning algorithm (InterPlanetary Support Vector Machine, IPSV, `https://pypi.org/project/ipsvm/`). Once a shock candidate was identified through one of the two methods, the authors required a set of upstream/downstream relations on the magnetic field plasma data to be satisfied in order to confirm that the candidate was indeed a shock.

TRUFLS, instead, looks where such jump conditions are satisfied using a moving average scanning the entire timeseries that is required to analyse. The conditions to be satisfied to identify a shock event

are the following:

$$\frac{B_d}{B_u} \geq 1.2 \tag{1}$$

$$\frac{n_d}{n_u} \geq 1.2 \tag{2}$$

$$\text{FF}: \quad V_d - V_u \geq 20\ \text{km/s} \tag{3}$$

$$\text{FR}: \quad V_u - V_d \geq 20\ \text{km/s} \tag{4}$$

Here, the subscripts u and d indicate upstream and downstream averages respectively, and B and V denote the magnetic field magnitude and SC-frame plasma flow speed, respectively. Equations (1) and (2) represent the compression of magnetic field and plasma density expected at the shock, respectively. The criterion on the plasma bulk flow speed for the Fast Forward (FF) and Fast Reverse (FR) cases are summarised in Equations (3) and (4), respectively. We restrict our analyses on fast shocks (i.e., shocks for which the shock speed is larger than the upstream fast magnetosonic speed). Vice versa, slow shocks are not treated here. It is worth underlining that in the ipshocks.fi database, a further constraint is requested to confirm that the candidate event is indeed a shock, namely the proton temperature jump $T_d/T_u \geq 1.2$. Within our identification, we relax this request, due to the fact that temperature data are the ones with the highest levels of noise.

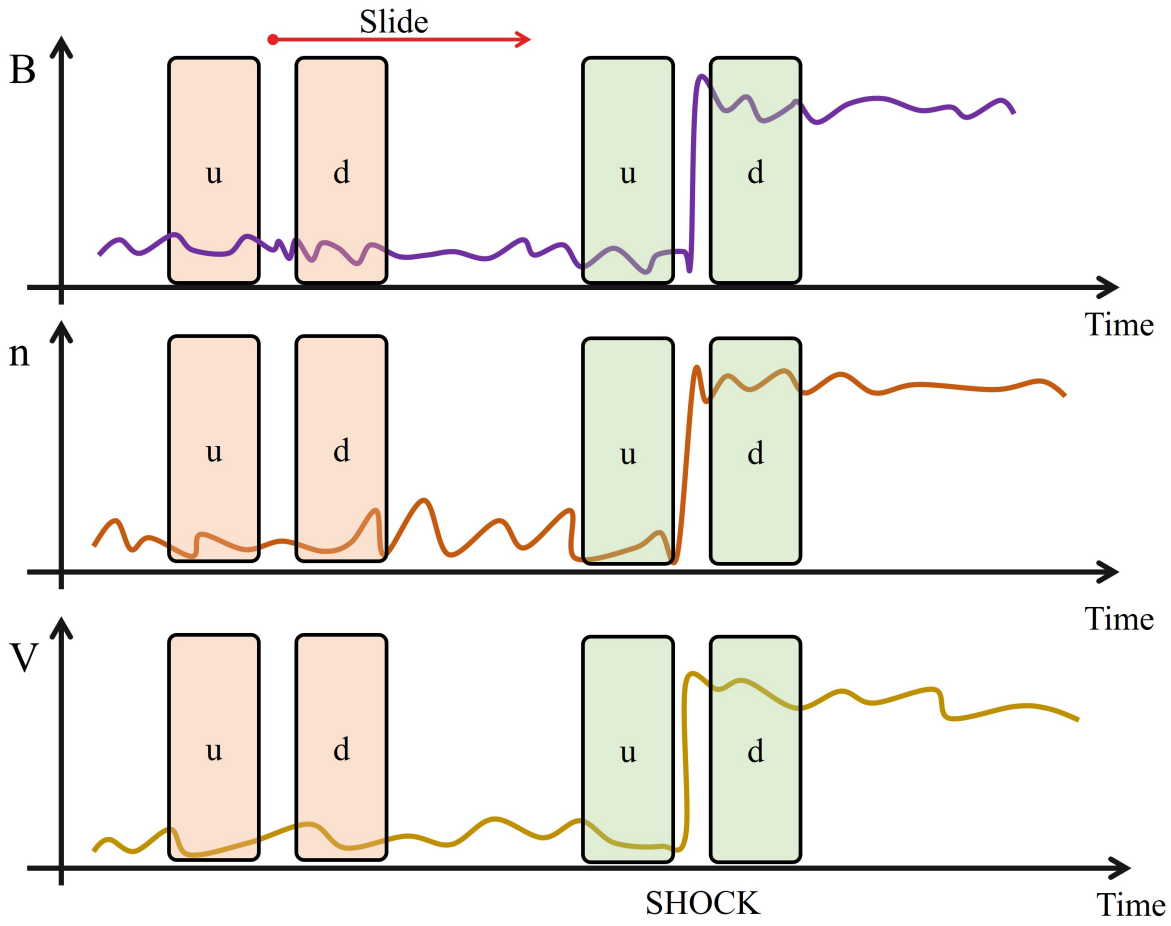

Figure 2: Sketch showing the sliding average windows (u and d, shaded panels) identifying a Fast Forward shock (green) as done in the TRUFLS code.

The TRUFLS code searches for times where Equations (1–4) are verified in time series containing

magnetic field and plasma data. Upstream and downstream averaging windows (and an exclusion zone where the shock itself will be) are chosen, with their length being a user-defined parameter. The output of the code consists of the times when the jump conditions are satisfied, that therefore constitute the shock candidates. The process by which TRUFLS operates is further elucidated in Figure 2, where a sketch of a FF shock signature is reproduced together with the sliding averaging windows. Once candidates are identified and confirmed visually, the shock time is added to the in-situ shock catalogue, and the data pipeline proceeds to the shock characterisation, as discussed in Section 3.

It is worth underlining that when plasma data is not available, such diagnostics become more complex. While we developed a TRUFLS version working on magnetic field only candidates, that flags a lot of false positives, as Equation (1) is easily satisfied also at structures that are not shocks. For this reason, to automatically identify shocks the presence of plasma and magnetic field data is required.

2.2 Other shock identifications

The shock lists presented here are built mainly using the TRUFLS code, but also other means of identifications are used to make sure that the list is complete and up to date. To this end, magnetic field only candidates are often spotted by visual inspection and flagged in the list as "magnetic field only". Furthermore, we decided to coordinate and cross-check our shock list with the Interplanetary Coronal Mass Ejection (ICME) catalog "ICMECAT" built within the HELIO4CAST project, accessible here: `https://helioforecast.space/`. IP shocks identified through this cross-checking are flagged in our list, to facilitate the community to develop cross-project and cross-disciplinary efforts. For Wind events, our results are cross-checked with the Harvard and Smithsonian Center for Astrophysics Interplanetary Shock Database for Wind (`https://lweb.cfa.harvard.edu/shocks/`). Shocks that crossed PSP are not included in this catalog, as they are reported in the SODA PSP catalog at `https://parker.gsfc.nasa.gov/shocks.html`.

3 In-situ shock characterisation

Once an event is added to the shock catalog, it is characterised with a thorough shock parameter estimation (see Figure 1). For the SolO events, the presence of wave and particle foreshocks is also addressed and, when present further information about their features provided too. Below, we detail how shock parameters are computed in the catalog (Section 3.1, closely following Trotta et al. (2022)). The methodology yielding the enhanced information about particles and waves behaviour at SolO is dicussed in Section 3.2.

3.1 Shock parameter estimation techniques

In this Section we report the shock parameter estimation used for the cycle 25 shock list. We closely follow the related publication Trotta et al. (2022). For a synthetic description of the parameters provided, see Section 4.

It is well-known that the overall behaviour and structuring of collisionless shocks has several controlling parameters, determining how the energy is processed across the shock transition. The shock structure and behaviour is regulated by several parameters, the most important being the angle between the shock normal direction and the upstream magnetic field θ_{Bn}. For θ_{Bn} values close to 90°, i.e, when the upstream magnetic field is almost tangential to the shock surface, the shock is quasi-perpendicular. On the other hand, for θ_{Bn} values close to 0° (corresponding to an upstream magnetic field almost normal to the shock surface), the shock is quasi-parallel. Particle reflection and propagation far upstream is favoured at quasi-parallel shocks (Kennel et al. 1985), introducing the possibility for reflected particles to interact with the upstream plasma over long distances, creating unstable distributions and a collec-

tion of disturbances in the plasma properties, giving rise to the so-called particle and wave foreshocks. Other important parameters for the shock behaviour are the shock Alfvénic and fast magnetosonic Mach numbers, i.e., the ratio between the shock speed in the upstream flow frame (v_{sh}) and the upstream Alfvén (v_A) and fast magnetosonic (v_{fms}) speeds, respectively ($M_A \equiv v_{sh}/v_A$ and $M_{fms} \equiv v_{sh}/v_{fms}$) (see Burgess & Scholer 2015, for an extensive review). Another important parameter is the upstream plasma beta, defined as the ratio between and often the plasma and magnetic field pressure, often expressed as a ratio of squared thermal and Alfvén speeds $\beta \equiv v_{th}^2/v_A^2$. Finally, gas and magnetic compression ratios ($r_{Gas} \equiv n_d/n_u$ and $r_B \equiv B_d/B_u$, respectively) are also important to address shock behaviour.

Many different techniques have been used to address the above parameters using a single SC crossing the shock front, an often challenging task due to the microinstabilities and fluctuations typical of shock front transition. The techniques used throughout this work are summarised by Paschmann & Schwartz (2000), and also in Trotta et al. (2022), to which we refer the readers in need for a recap.

Here, we report on an advancement made within the SERPENTINE project for the use of such single-SC shock parameter estimation techniques. Part of the below discussion is also in Trotta et al. (2022).

The premise is that most shock parameter estimation techniques from SC data involve an operation of averaging plasma quantities upstream/downstream of the shock crossing, making the results particularly sensitive to the choice of averaging windows. We build on the idea to adopt an ensemble-based approach for such choices of averaging windows first suggested by Balogh et al. (1995), looking at magnetic field Ulysses observations of IP shocks.

To introduce and show a controlled test for our approach, a synthetic SC measurement was generated using the Rankine-Hugoniot jump conditions, consequence of MagnetoHydroDynamics (MHD) conservation laws across a discontinuity (see Paschmann & Schwartz 2000; Trotta et al. 2022).

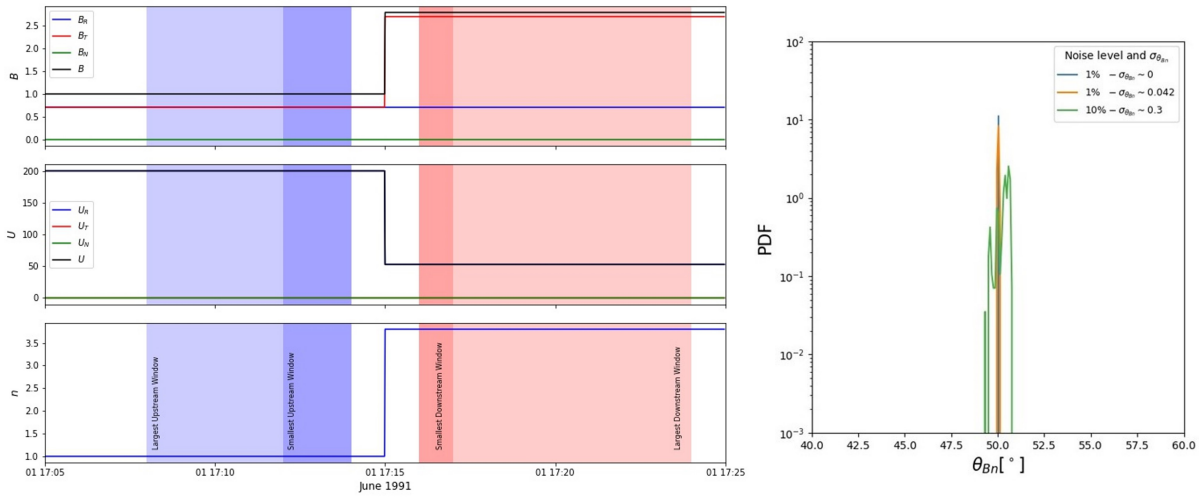

Figure 3: *Left*: Synthetic measurements for a Rankine-Hugoniot compliant shock with θ_{Bn}= 50° and gas compression ratio $r_{gas} = 3.8$. Panel show magnetic field magnitude and components (top), plasma bulk flow speed (middle) and density (bottom). The blue (red) shaded areas highlight the windows chosen for upstream(downstream) averaging. *Right*: PDF distributions of $\theta_{Bn}$for three shocks with the same nominal geometry and different levels of added noise. *Figure adapted from Trotta et al. (2022).*

Such synthetic measurements are shown in the right-hand side panel of Figure 3, where a Rankine-Hugoniot compliant shock with $\theta_{Bn} = 50^\circ$ and gas compression ratio $r_{gas} = 3.8$ is represented. As it can be seen from magnetic field, bulk flow speed and density time-series measurements (Figure 3(a)-(c)), the shock transition is such that the upstream is on the left-hand side of the Figure, i.e. before 17:15 of 1 June 1991, and the downstream is represented by the timeseries after 17:15 (obviously, time here has no physical meaning).

The parameter estimation is performed as follows: a smallest possible averaging window is chosen for upstream and downstream. Given the discussion about the Rankine–Hugoniot relations assuming the shock transition as infinitesimal, the idea is to choose such windows as close as possible to the shock front, without including it in the averaging process. Care must be taken in excluding also the shock foot in the very close upstream, as well as the downstream overshoot. When applying these diagnostics, as it will be discussed later concerning real observations, the choice for smallest/largest upstream window will depend on many different factors, e.g., the amount of disturbances that may be present upstream/downstream of the shock and the resolution available for the measurements.

In the left hand side panels of Figure 3, the smallest upstream (downstream) averaging windows are shown with the dark shaded blue (red) panels. Then, after choosing an appropriate cadence, the smallest averaging windows are extended to the largest, and overlapped with the smallest windows. For each couple of upstream/downstream windows, a shock normal (and subsequently $\theta_{\rm Bn}$ value) is evaluated. In this way, an ensemble of shock parameters is computed, and it is possible to address the robustness of the parameters estimation by looking at how is the ensemble distributed, as we shall see below. Note that, since we add duration to the smallest upstream/downstream windows, the measurements close to the shock are counted multiple times, ensuring that the calculation is carried out as close as possible to the shock front at all times. In the cycle 25 shock list, for each event, the smallest (largest) averaging windows are fixed at four (eight) minutes, compatible with the choice carried out in the shock catalogue `http://ipshocks.fi`.

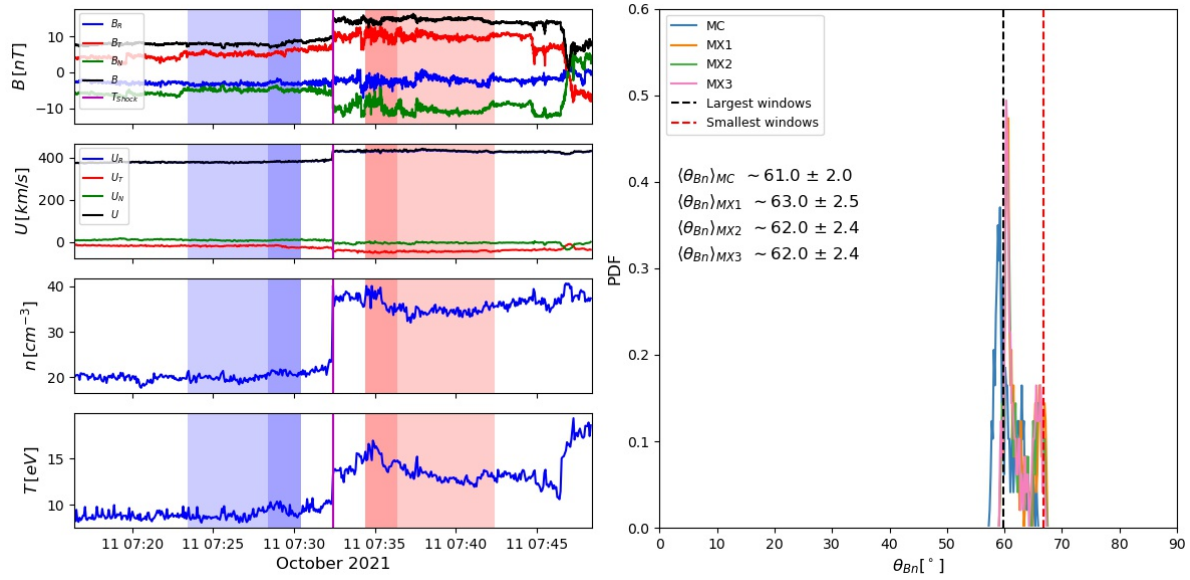

Figure 4: The event of October 11, 2021, as seen by Solar Orbiter. The left-hand panels show magnetic field B, ion bulk flow U, ion density n and temperature T measured by the MAG and SWA instruments. Vector quantities are shown in the RTN coordinate system. The blue/red shaded panels show the smallest (dark) to largest (lighter) averaging windows in the upstream/downstream regions. The vertical purple line shows the shock crossing time. The right-hand side panel shows the PDF distribution of $\theta_{\rm Bn}$ values obtained for this event, with the vertical red (blue) dashed line showing the parameter esimation using the smallest (largest) window choice. The average values of $\theta_{\rm Bn}$ obtained with each technique are also shown. *Figure from Trotta et al. (2022).*

The shock geometry was then computed on the synthetic signal using the Mixed Mode (MX) 3 method (see Deliverable D4.1 or Paschmann & Schwartz 2000) and about 1000 different combinations of upstream/downstream windows. The results of this experiment are reported in Figure 3 (right), where the probability density functions (PDFs) for the computed $\theta_{\rm Bn}$ values are shown. The three PDF correspond to three different levels of white noise introduced in the signal, mimicking real measurements. Such PDFs,

as expected, are peaked at the nominal θ_{Bn} value of 50° for each case. It can also be seen that when noise is added, the PDF distribution of θ_{Bn} values broadens, as it is particularly evident for the 10% noise level case (green line in Figure 3, right). Another interesting feature of this method is that it is possible to characterise the spread of this PDFs computing, together with the average value, $\langle\theta_{Bn}\rangle$, and its standard deviation $\sigma_{\theta_{Bn}}$, which becomes a measure for the sensitivity of the parameter estimation to the choice of upstream/downstream window and, in other words, an uncertainty for the parameter estimation. It is possible to note that the broadening observed here is rather small (with a maximum discrepancy of about 1 degree from the nominal shock geometry), due to the fact that the averaging process averages out the white noise.

Finally, a real case for such a shock characterisation, for a real event in the Work Package (WP)4 list is shown. Figure 4 shows an overview for the quiet event, with ∼30 minutes of SC data. The shock transition, highlighted by the vertical magenta line in the Figure, appears well-behaved, without strong upstream/downstream structuring. In particular, low levels of upstream/downstream fluctuations make this a good observational case for the systematic shock parameters estimation method.

The parameter estimation reveals that the shock geometry is quasi-perpendicular, with $\langle\theta_{Bn}\rangle \sim 60°$. This has been obtained using smallest averaging windows of about 2 minutes upstream and downstream, and largest windows of about 10 minutes. This choice is such that the time window over which the average is taken is always larger than kinetic timescales (Ω_{ci}^{-1} is of order ~ 10 s), making sure that the MHD description on which the data analysis technique rely is appropriate. As stated above, other studies looking at IP shock statistics and catalogues have analogous choices for upstream/downstream windows. The upstream/downstream averaging windows have been broadened with timesteps of 16 seconds, larger than the resolution of the SolO plasma instrument. As it can be seen from the right-hand side panel of Figure 4, the PDF distribution of θ_{Bn} values is strongly peaked, with a small value of $\sigma_{\theta_{Bn}} \sim 2$. Furthermore, we find strong agreement between the results obtained using different techniques Magnetic Coplanarity (MC) and MX1–2–3 for the shock normal evaluation. These results indicate that the parameter estimation for this shock transition is particularly robust, i.e., it has weak dependence on the choice of upstream/downstream averaging windows.

3.2 Waves and particles characterisation

In the SolO shock list, we characterise the behaviour of the plasma interacting with IP shock waves. The detailed characterisation of waves and energetic particle properties is carried out for all the cases in the SolO catalogue, and for selected events in the multi-SC list. This topic is particularly interesting as IP waves and particle foreshocks are much less well-characterised than the foreshocks upstream of Earth's bow shock (see Kajdič et al. 2012 and Blanco-Cano et al. 2016 for the IP case, and Wilkinson 2003 for a review on Earth's bow shock foreshocks).

The wave activity upstream of each shock is characterised using different methods. We compute the value of magnetic field fluctuations upstream, and report it in the list, as $\delta B/B_0 = |\mathbf{B}(t+\tau) - \mathbf{B}(t)|/|\mathbf{B}_0|$, where τ has been chosen to be of 1 minute. The mean upstream $\delta B/B_0$ value is reported in the list. Such information is also be provided to the user as a quicklook plot.

Quicklook plots of wavelet spectrograms of magnetic field intensity B and trace spectrogram of the magnetic field components are included in the list. Finally, to gain insights about the polarisation of the waves observed, the reduced magnetic helicity, normalised by the power in magnetic field fluctuations $\sigma_m(k) \equiv kH_m^{(r)}(k)/E_B(k)$ (where k is the wavenumber, $H_m^{(r)}(k)$ is the reduced magnetic helicity (Matthaeus et al. 1982) and $E_B(k)$ is the magnetic power spectral density) is also shown.

An example of such a foreshock characterisation is presented in Figure 5, where the wave behaviour upstream of the strong shock of October 30th has been characterised. The magnetic fields components in RTN coordinates are shown to help the user in the visual identification of interesting features in the magnetic field signatures, including the presence of structures and rotation. The level of fluctuations in

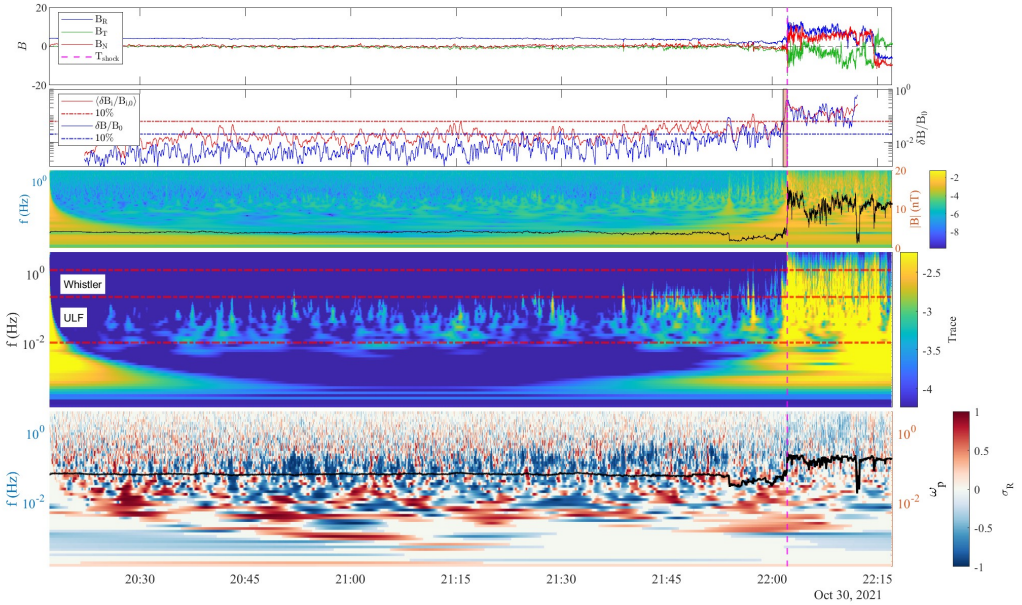

Figure 5: Characterisation of the waves upstream of the October 30th event. For a two-hour interval, we report, from top to bottom, the magnetic field components in RTN coordinates, the level of fluctuations in the components and magnitude of magnetic field with their 10% levels with respect to the maximum just upstream of the shock (red and blue and horizontal lines, respectively); wavelet spectrogram of magnetic field intensity (color) and magnetic field magnitude (black line); Trace wavelet spectrogram with whistler and ULF frequency ranges as reported in Blanco-Cano et al. (2016); reduced magnetic helicity σ_m (color) and ion plasma frequency ω_p (black line).

the components and magnitude of magnetic field with their 10% levels with respect to the maximum just upstream of the shock is then shown to help characterise a rise in wave activity upstream of the shock. It may be seen that, in the case shown in Figure 5 has no strong wave activity upstream, even though a trend may be identified in the $\sim$ 15 minutes upstream of the shock. The wavelet spectrogram of magnetic field intensity (color) confirms this scenario, as not many compressive fluctuations are found and the wavelet spectrogram is dominated by the presence of the shock (see the corresponding signal at the shock time, marked by the magenta line). The trace wavelet spectrogram reveals some wave activity in the shock upstream. In the corresponding panel, the whistler and Ultra Low Frequency (ULF) frequency ranges are highlighted by the horizontal red lines, to evaluate wave activity in the high and low frequency regimes (see Wilson et al. 2009). Finally, looking at the reduced magnetic helicity σ_m (color), we find no strong signature in wave polarisation near the shock. $\sigma_m < 0$ (blue) indicates left-hand polarisation, while $\sigma_m > 0$ (red) indicates right-hand polarisation (in the SC frame). From Figure 5, it is possible to see waves with left-hand polarisation far upstream of the shock, possibly a feature of the solar wind where the shock is propagating.

The features of particle foreshocks are also characterised for the SolO events. Quicklook plots and information about length of particle foreshock as well as particle response to the IP shock passage are included in the list. An example of such an investigation for the October 30th event is shown in Figure 6, where the capabilities of the EPD suite are highlighted. Here, proton intensity spectrograms are reported with resolution of about a second in the 0.01–100 MeV energy range. In Figure 6 it is possible to see a particle foreshock extending for up to 45 minutes upstream (see, in particular, the SupraThermal Protons and alpha (STEP) signal).

To go beyond this somewhat qualitative characterisation of particle foreshocks, information about intensity-time profiles in selected energy channels is also provided for the SolO list and for selected

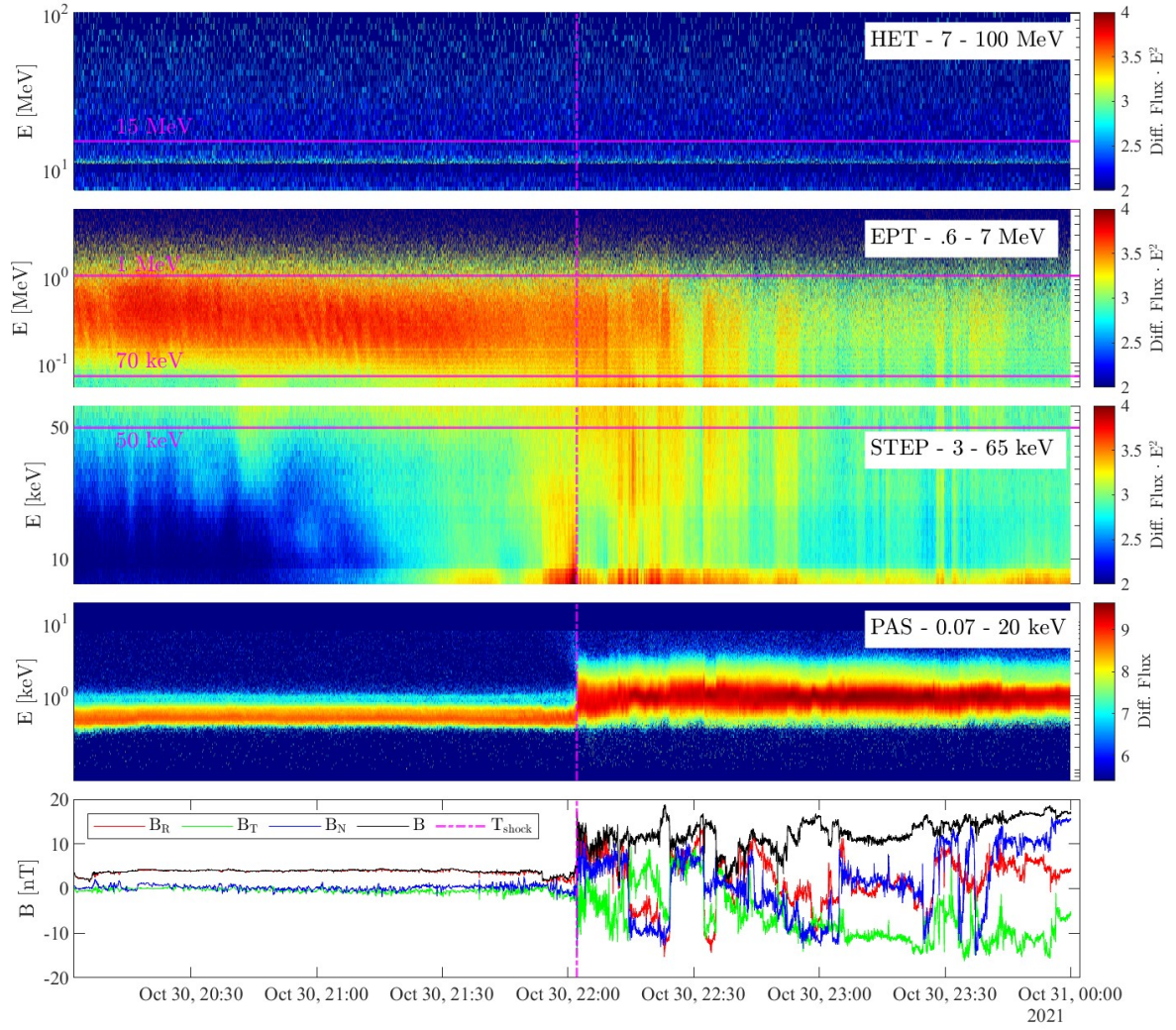

Figure 6: Characterisation of the particle behaviour for the October 30th event. From top to bottom, we report particle intensity spectrograms for the HET, EPT and STEP sensors on the SolO / EPD suite; energy flux obtained from the SolO / SWA / PAS instrument, showing the thermal particle population; magnetic field data from SolO / MAG. The shock transition is highlighted by the dashed magenta line.

candidates in the multi-SC list, as per Deliverable D4.1. This is shown in Figure 7, where the profiles of particle fluxes in 15 MeV, 1 MeV, 70 keV and 50 keV are shown. Note that these are also highlighted in Figure 6 by the horizontal magenta lines.

The profiles are included in the list as quicklook plots. Furthermore, the particle behaviour is listed as “spike”, “plateau”, “structured/irregular”, “no response”, summarised in the sketch reported in Figure 8. When no particles are found at the energies mentioned, the event is flagged with “zero flux” for what concerns that energy channel. Such behaviour of particle response to the presence of an IP shock is important to constrain the behaviour of energetic particles. Similar efforts have been done for previous Solar Cycles (e.g. Lario et al. 2003), making this one particularly interesting due to the novel energy-time resolution capabilities provided by the SolO EPD suite. We also include in the list the time difference between the peak of energetic particles and the shock passage time, indicating with negative, zero and positive values the cases when the peak in particle intensity occurs before, at and after the shock passage, aiming to find the conditions responsible for this difference. This information is very valuable, due

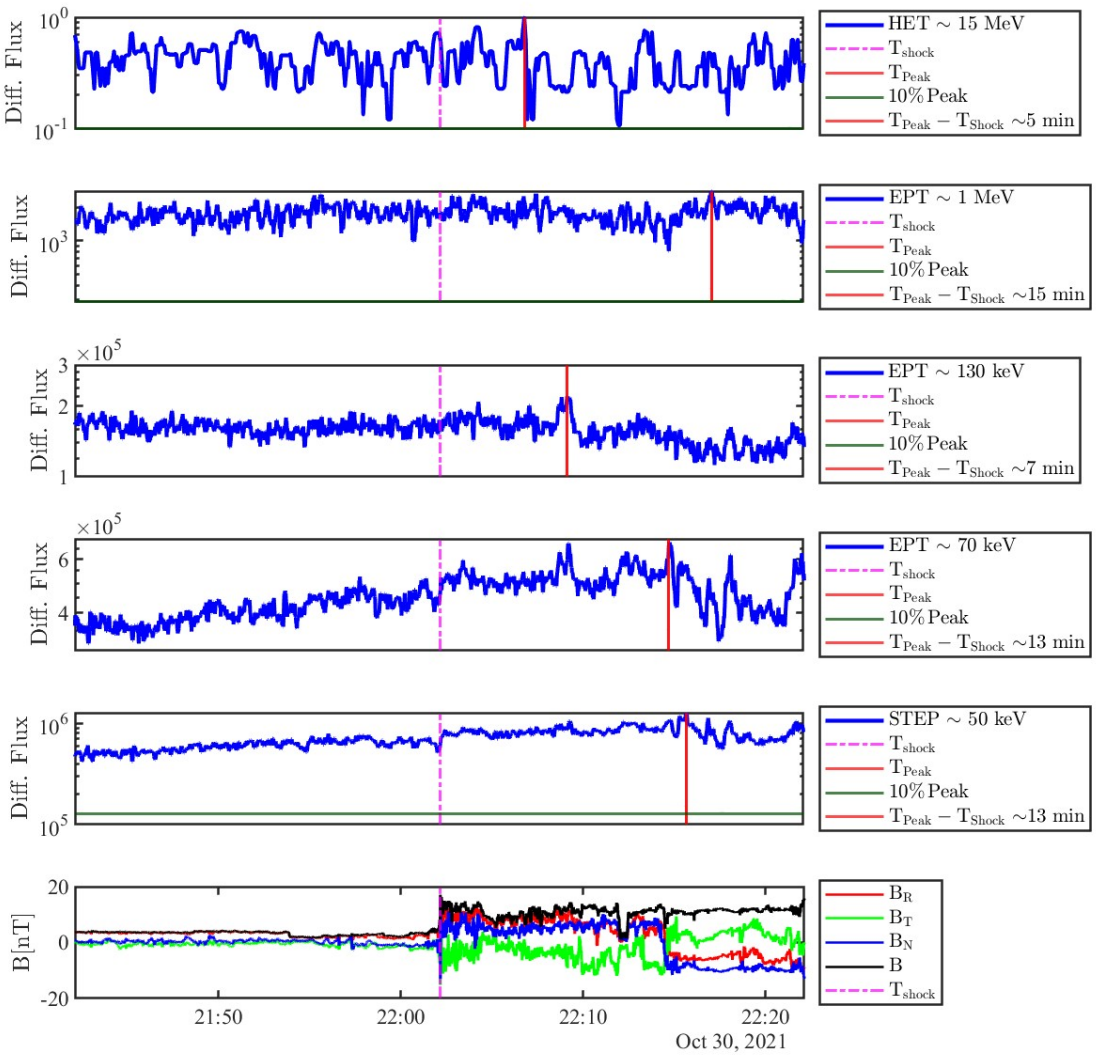

Figure 7: Time-intensity profiles for protons at, from top to bottom, 15 MeV, 1MeV, 130 keV, 70 keV and 50 keV. In the bottom panel is shown the magnetic field profile. the magenta line indicates the shock passage and the red vertical lines indicate the time at which particle intensities peak.

to the fact that particle fluxes are expected to peak at the shock, but recent evidences suggest that this is not often the case, with important implications on the particle acceleration mechanisms at play (see Kartavykh et al. 2016, for example).

4 Structure of the shock lists

Table 1 summarises the parameters provided for the multi-SC list, while Table 2 summarises the extra information provided for SolO shocks. In the SolO shock list, we decided to report on energetic particle response for each event in 5 different energy ranges, namely 50 keV, 70 keV, 130 keV, 1 MeV, 15 MeV (thus utilising the full EPD suite on-board SolO). All these data products are available at `https://data.`

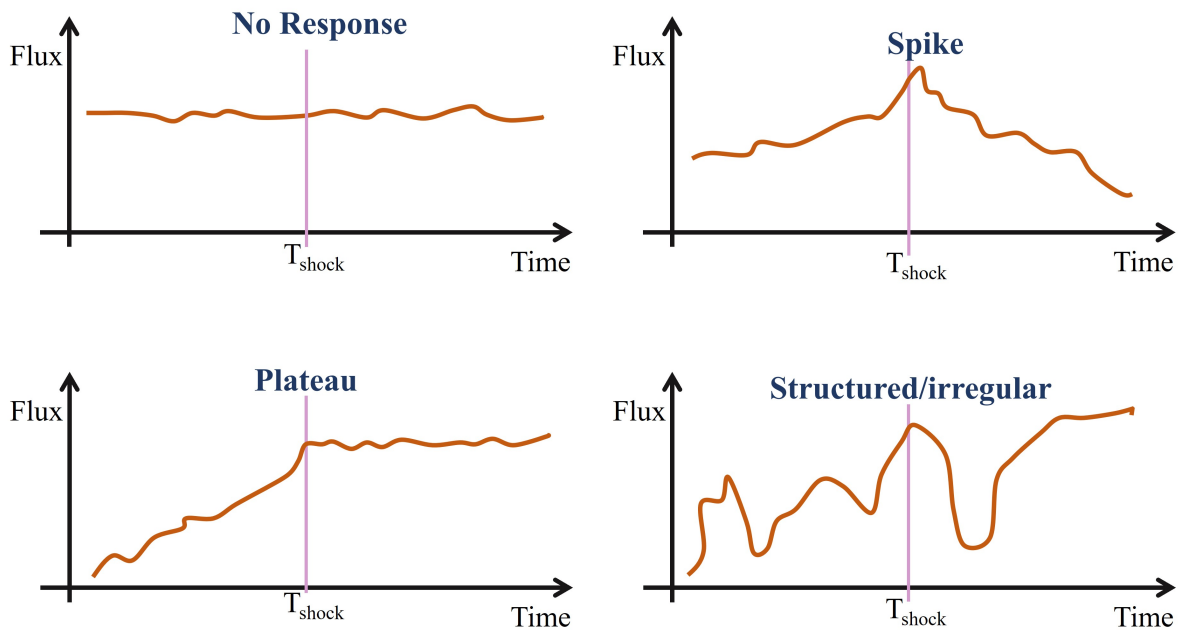

Figure 8: Sketch of the type of energetic particle flux responses to the IP shock passage.

serpentine-h2020.eu.

Parameter	Content	Units	Notes
Shock ID	Shock unique identifier	-	-
Shock Date	Date of Shock Observation	UT	-
Shock Time	Time of the shock crossing	UT	-
Spacecraft	Name of spacecraft	-	-
Heliocentric distance	Distance from the Sun	AU	-
Solar-MACH config	Link to multi-SC configuration plot	-	-
Associated WP2 event	ID of associated WP2 SEP event	-	-
Spacecraft	Name of spacecraft	-	-
Mean upstream $\delta B/B_0$	$\delta B/B_0$ (lag: 1 min)	-	Avgerage Window: 8 min
Upstream density	Mean upstream ion density	cm^{-3}	Avgerage Window: 8 min
Upstream β	Mean upstream plasma beta	-	Avgerage Window: 8 min
Upstream $\mathbf{B}$	Mean upstream $\mathbf{B}$ vector	nT	Avgerage Window: 8 min
$\hat{\mathrm{n}}_{\mathrm{Shock}}$	Mean shock normal vector	-	Computed with MX3 or MC
θ_{Bn}	Mean shock normal angle	$^{\circ}$	-
$\mathrm{V}_{\mathrm{Shock}}$	Mean shock speed	$\mathrm{km/s}$	Along $\hat{\mathrm{n}}_{\mathrm{Shock}}$, in SC rest frame
M_{A}	Alfvénic Mach number	-	-
$\mathrm{M}_{\mathrm{fms}}$	Fast Magnetosonic Mach number	-	-
r_{B}	Mean magnetic compression ratio	-	-
$\mathrm{r}_{\mathrm{Gas}}$	Mean gas compression ratio	-	-
Structures - two hours	Structuring across shock	-	Yes/No
Notes	E.g., data availability	-	-
Identified with	E.g., TRUFLS, Visual inspection	-	-

Table 1: The multi-SC list. Shock normal vector, θ_{Bn}, shock speed and compression ratios are computed using SerPyShock with upstream/downstream windows in a range between 6 and 10 minutes. The orbit plots are provided using the online capabilities of the Solar-MACH tool (Gieseler et al. 2023). MX3 stands for "Mixed Mode 3" method while MC stands for "Magnetic Coplanarity" methods (see D4.3).

Parameter	Content	Units	Notes
Set of shock parameters	As in Table 1	-	-
Structures - 8 minutes	Structuring across shock	-	Yes/No
Possibility of Multi-SC observation	Other SC within 0.2 Astronomical Unit (AU)	-	-
Wave foreshock	Present	-	Yes/No
Foreshock extent	Duration of wave foreshock	minutes	-
Frequency range	Frequencies of enhanced wave activity	Hz	-
Low energy particle reflection	Present	-	Yes/No
Proton response at selected energies	No response/Spike/Plateau/Irregular (Fig. 8)	-	-
Proton peak delay $\mathrm{t}_{\mathrm{peak}} - \mathrm{t}_{\mathrm{shock}}$	For selected energies	minutes	-
Electron response at selected energies	Present/which energies	-	-
Electron peak delay $\mathrm{t}_{\mathrm{peak}} - \mathrm{t}_{\mathrm{shock}}$	For selected energies	minutes	-
Notes on particle response	-	-	

Table 2: The extra information provided in the SolO list.

Bibliography

Balogh, A., Gonzalez-Esparza, J. A., Forsyth, R. J., et al. 1995, Space Sci. Rev., 72, 171

Blanco-Cano, X., Kajdič, P., Aguilar-Rodríguez, E., et al. 2016, Journal of Geophysical Research: Space Physics, 121, 992

Burgess, D. & Scholer, M. 2015, Collisionless Shocks in Space Plasmas (Cambridge University Press)

Gieseler, J., Dresing, N., Palmroos, C., et al. 2023, Frontiers in Astronomy and Space Sciences, 9

Kajdič, P., Blanco-Cano, X., Aguilar-Rodriguez, E., et al. 2012, Journal of Geophysical Research: Space Physics, 117

Kartavykh, Y. Y., Dröge, W., & Gedalin, M. 2016, The Astrophysical Journal, 820, 24

Kennel, C. F., Edmiston, J. P., & Hada, T. 1985, A Quarter Century of Collisionless Shock Research (American Geophysical Union (AGU)), 1–36

Kilpua, E. K., Lumme, E., Andreeova, K., Isavnin, A., & Koskinen, H. E. 2015, Journal of Geophysical Research: Space Physics, 120, 4112

Lario, D., Ho, G. C., Decker, R. B., et al. 2003, in American Institute of Physics Conference Series, Vol. 679, Solar Wind Ten, ed. M. Velli, R. Bruno, F. Malara, & B. Bucci, 640–643

Matthaeus, W. H., Goldstein, M. L., & Smith, C. 1982, Phys. Rev. Lett., 48, 1256

Paschmann, G. & Schwartz, S. J. 2000, in ESA Special Publication, Vol. 449, Cluster-II Workshop Multiscale / Multipoint Plasma Measurements, ed. R. A. Harris, 99

Trotta, D., Vuorinen, L., Hietala, H., et al. 2022, Frontiers in Astronomy and Space Sciences, 9

Wilkinson, W. P. 2003, Planetary and Space Science, 51, 629, collisionless Shocks

Wilson, L. B. I., Cattell, C. A., Kellogg, P. J., et al. 2009, Journal of Geophysical Research: Space Physics, 114